Journal of Sound and Vibration (2000) **236**(4), 705–724
doi:10.1006/jsvi.2000.3021, available online at http://www.idealibrary.com on IDEAL®

IDENTIFICATION OF VEHICLE AXLE LOADS FROM BRIDGE DYNAMIC RESPONSES

X. Q. Zhu and S. S. Law

Civil and Structural Engineering Department, Hongkong Polytechnic University, Hung Hom, Hong Kong, People's Republic of China

(*Received* 12 *October* 1999, *and in final form* 30 *March* 2000)

A method is presented to identify moving loads on a bridge deck modelled as an orthotropic rectangular plate. The dynamic behavior of the bridge deck under moving loads is analyzed using the orthotropic plate theory and modal superposition principle, and Tikhonov regularization procedure is applied to provide bounds to the identified forces in the time domain. The identified results using a beam model and a plate model of the bridge deck are compared, and the conditions under which the bridge deck can be simplified as an equivalent beam model are discussed. Computation simulation and laboratory tests show the effectiveness and the validity of the proposed method in identifying forces travelling along the central line or at an eccentric path on the bridge deck.

1. INTRODUCTION

Information of vehicular load on a bridge deck is essential to bridge design as it constitutes the live load component in the bridge design code. Traditionally, the vehicular load is either measured directly from an instrumented vehicle [1, 2] or computed from models of the bridge deck and the vehicle [3–5]. It would be very expensive and the results obtained are subjected to bias in the first approach, while the second approach is subjected to modelling errors. Systems have been developed for weigh-in-motion of the vehicles [6, 7], but they all measure only the static axle loads. All the weigh-in-motion techniques treat the bridge and vehicle in a two-dimensional problem. A technique to estimate the vehicular loads from the vibration responses of the bridge deck is required such that the different parameters of the bridge and vehicle system are accounted for in the measured responses, and the cost involved would be much less than that by direct measurement.

O'Connor and Chan [8] developed a method to identify the vehicle–bridge interaction force, in which the bridge is modelled as an assembly of lumped masses interconnected by massless elastic beam elements. Law *et al.* [9] modelled the bridge deck as a simply supported Euler beam. The interaction forces are represented as step functions in a small time interval. The moving forces are then identified using the modal superposition principle in time domain. Later, Law *et al.* [10] performed Fourier transformation on the equations of motion which are expressed in modal co-ordinates. The relation between the responses and the forces is obtained in frequency domain. The time histories of the forces are found by the least-squares method. Chan *et al.* [11] used an Euler beam to model the bridge deck in the interpretation of dynamic loads crossing the deck. The Euler beam theory together with modal analysis is used to identify moving loads from the bridge responses. Law and Fang [12] also reported a state estimation approach in which the state-space formulation of the

0022-460X/00/390705 + 20 $35.00/0

dynamic system is solved using dynamic programming with minimization of the errors between the measured and the reconstructed responses from the identified moving forces. Another method based on the modal superposition and optimization technique is also developed by Zhu and Law [13] to identify a group of moving forces in the time domain. The bridge deck is modelled as a multi-span continuous Timoshenko beam with non-uniform cross-section, and the forces are modelled as a group of moving loads.

All the above works are based on the bridge–vehicle interaction with a simply supported beam. A beam model cannot truly represent the three-dimensional behavior of the bridge deck in practice, particularly when a vehicle travels not along the centerline of the bridge deck. Since many types of bridge decks, including those of slab bridges, hollow-core slab bridges, and deck and girder bridges can be effectively modelled by an isotropic or orthotropic plate [14], identification of the real interaction forces is possible and feasible.

The bridge deck is modelled as a simply supported orthotropic rectangular plate in this study. Dynamic behavior of the bridge deck under moving loads is analyzed using the orthotropic plate theory and modal superposition. A moving load identification method based on a regularization procedure is developed, and the solutions are obtained in time domain. The conditions under which the bridge deck can be simplified as an equivalent beam are discussed, and the identification of eccentric travelling loads is presented. Computational simulation and laboratory test results are given to illustrate application of the proposed method to identify a two forces system.

2. FREE VIBRATION OF A PLATE

The problem of a plate under the action of moving forces attracted much research attention only in the last two decades. Fryba [15] has solved analytically the dynamic responses of uniform flat plate under a moving load along a specified path. Wu *et al.* [16] analyzed the dynamic responses of a flat plate subjected to various moving loads by the finite element method. Later, Wang and Lin [17] analyzed the dynamic behavior of a multi-span continuous Mindlin plate subjected to a moving load. Transfer matrix is used to determine the natural frequency and the vibration modes of the plate. Marchesiello *et al.* [18] analyzed the dynamics of multi-span continuous straight bridges subjected to multi-degrees-of-freedom (d.o.f.) moving vehicle excitation by applying the mode superposition principle. The modes are computed by means of the Rayleigh–Ritz method. Chan and Chan [19] analyzed the dynamic behavior of slab-on-girder bridges by eccentric beam elements. Zhu and Law [20] modelled the bridge deck as an orthotropic plate, and the dynamic behavior of the bridge deck under moving loads is analyzed basing on the modal superposition principle. A brief description of the plate model using in this paper is given below.

According to Huffington and Hoppmann [21], the governing equations of motion of an orthotropic plate shown in Figure 1 can be written as follows:

$$D_x \frac{\partial^4 w}{\partial x^4} + 2D_{xy} \frac{\partial^4 w}{\partial x^2 \partial y^2} + D_y \frac{\partial^4 w}{\partial y^4} + C \frac{\partial w}{\partial t} + \rho h \frac{\partial^4 w}{\partial t^2} = p, \tag{1}$$

where

$$D_{xy} = (D_x v_{yx} + 2D_k), \quad D_x = \frac{E_x h^3}{12(1 - v_{xy} v_{yx})}, \quad D_y = \frac{E_y h^3}{12(1 - v_{xy} v_{yx})}, \quad D_k = \frac{G_{xy} h^3}{12}.$$

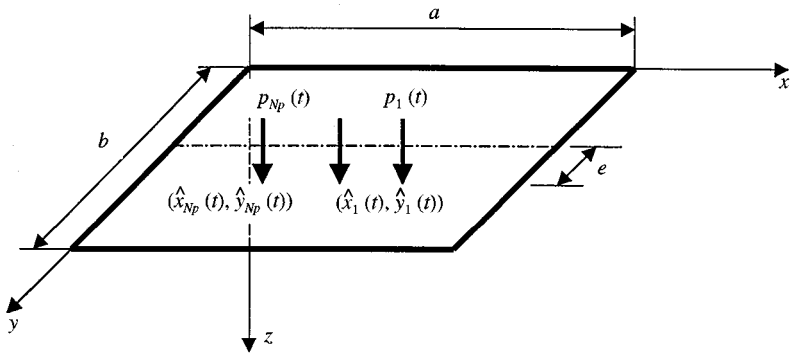

Figure 1. Orthotropic plate under moving loads.

D_x, D_y are the flexural rigidities of the orthotropic plate in the x and y directions respectively, D_k is the twisting rigidity of plate, C the damping coefficient, h the thickness of the plate, E_x, E_y are the modulus of the plate in the x and y directions respectively, v_{xy} the Poisson ratio associated with a strain in the y direction for a load in the x direction, G_{xy} the shear modulus, $p(x, y, t)$ the external transverse load, $w(x, y, t)$ the displacement of plate in the z direction and ρ the mass density of plate material.

The free vibration of the plate without damping is analyzed. Assuming the plate is simply supported along $x = 0$ and a with the other two sides free to vibrate. The displacement of the plate can be written as

$$w(x, y, t) = \sum_{m,n} Y_{mn}(y) \sin\left(\frac{m\pi x}{a}\right) \sin(\omega_{mn} t + \theta), \tag{2}$$

where ω_{mn} is the natural frequency corresponds to the mth mode in the x direction and the nth node in the y direction, θ the initial angle, and $Y_{mn}(y) \sin(m\pi x/a)$ the mode shape. Substituting equation (2) into equation (1), one has

$$D_y Y_{mn}^{(4)}(y) - 2D_{xy}\left(\frac{m\pi}{a}\right)^2 Y_{mn}^{(2)}(y) + \left[D_x\left(\frac{m\pi}{a}\right)^4 - \rho h \omega_{mn}^2\right] Y_{mn}(y) = 0. \tag{3}$$

The solution on $Y_{mn}(y)$ can be obtained [20] and classified as follows according to the properties of the plate.

(1) When $D_x < \rho h \omega_{mn}^2 (a/m\pi)^4$,

$$Y_{mn}(y) = A_{mn} \sin(r_{2mn} y) + B_{mn} \cos(r_{2mn} y) + C_{mn} \sinh(r_{1mn} y) + D_{mn} \cosh(r_{1mn} y), \tag{4}$$

where

$$r_{1mn} = \frac{m\pi}{a} \sqrt{\frac{D_{xy} + \sqrt{D_{xy}^2 + D_y \rho h \omega_{mn}^2 (a/m\pi)^4 - D_x D_y}}{D_y}},$$

$$r_{2mn} = \frac{m\pi}{a} \sqrt{\frac{-D_{xy} + \sqrt{D_{xy}^2 + D_y \rho h \omega_{mn}^2 (a/m\pi)^4 - D_x D_y}}{D_y}}. \tag{5}$$

(2) When $D_{xy}^2/D_y + \rho h\omega_{mn}^2(a/m\pi)^4 > D_x > \rho h\omega_{mn}^2(a/m\pi)^4$,

$$Y_{mn}(y) = A_{mn}\sinh(r_{1mn}y) + B_{mn}\cosh(r_{1mn}y) + C_{mn}\sinh(r_{3mn}y) + D_{mn}\cosh(r_{3mn}y), \quad (6)$$

where

$$r_{3mn} = \frac{m\pi}{a}\sqrt{\frac{D_{xy} - \sqrt{D_{xy}^2 + D_y\rho h\omega_{mn}^2(a/m\pi)^4 - D_xD_y}}{D_y}}. \quad (7)$$

(3) When $D_x > D_{xy}^2/D_y + \rho h\omega_{mn}^2(a/m\pi)^4$,

$$\begin{aligned} Y_{mn}(y) = {} & \cosh(r_{4mn}y)(A_{mn}\cos(r_{5mn}y) + B_{mn}\sin(r_{5mn}y)) \\ & + \sinh(r_{4mn}y)(C_{mn}\cos(r_{5mn}y) + D_{mn}\sin(r_{5mn}y)), \end{aligned} \quad (8)$$

where

$$r_{4mn} = \frac{m\pi}{a}\sqrt{\frac{1}{2}\left(\frac{D_{xy}}{D_y} + \sqrt{\frac{D_x}{D_y} - \frac{\rho h\omega_{mn}^2}{D_y}\left(\frac{a}{m\pi}\right)^4}\right)},$$

$$r_{5mn} = \frac{m\pi}{a}\sqrt{\frac{1}{2}\left(-\frac{D_{xy}}{D_y} + \sqrt{\frac{D_x}{D_y} - \frac{\rho h\omega_{mn}^2}{D_y}\left(\frac{a}{m\pi}\right)^4}\right)}. \quad (9)$$

The parameters $A_{mn}, B_{mn}, C_{mn}, D_{mn}$ and the natural frequencies are determined from the free boundary conditions at $y = 0$ and b. The edge moment, the transverse shear and the torsional moment are zero at these edges, giving

$$\begin{aligned} \frac{\partial^2 w}{\partial y^2} + \nu_{xy}\frac{\partial^2 w}{\partial x^2} &= 0, \\ -D_{xy}\frac{\partial^3 w}{\partial x^2\,\partial y} - D_y\frac{\partial^3 w}{\partial y^3} &= 0, \\ 2D_k\frac{\partial^3 w}{\partial x^2\,\partial y} &= 0, \\ -D_{xy}\frac{\partial^3 w}{\partial x^2\,\partial y} - D_y\frac{\partial^3 w}{\partial y^3} - 2D_k\frac{\partial^3 w}{\partial x^2\,\partial y} &= 0. \end{aligned} \qquad (y = 0 \text{ or } y = b) \quad (10)$$

Substituting equation (2) and equations (4)–(9) into equation (10), the following equation can be obtained:

$$\mathbf{A}\{\mathbf{C}\} = 0, \quad (11)$$

where $\mathbf{A}$ is a coefficient matrix $\{a_{ij}\}$ detail formulation of each coefficient are listed in Appendix B for the different classifications presented above, and $\{\mathbf{C}\} = \{A_{mn}\ B_{mn}\ C_{mn}\ D_{mn}\}^{\mathrm{T}}$.

Since only the non-zero solution of equation (11) is of interest, the determinant of the coefficient matrix is set equal to zero from which the natural frequencies

ω_{mn} $(m = 1, 2, \ldots; n = 1, 2, \ldots)$ are obtained. Vector $\{\mathbf{C}\}$ can then be obtained for each natural frequency, and hence $Y_{mn}(y)$ can be found.

3. DYNAMIC BEHAVIOR UNDER MOVING LOADS

The equations of motion of the orthotropic plate under moving loads expressed in equation (1) can be written as follows by expressing the force p as a time step function:

$$D_x \frac{\partial^4 w}{\partial x^4} + 2D_{xy} \frac{\partial^4 w}{\partial x^2 \partial y^2} + D_y \frac{\partial^4 w}{\partial y^4} + C \frac{\partial w}{\partial t} + \rho h \frac{\partial^2 w}{\partial t^2} = \sum_{l=1}^{N_p} p_l(t)\, \delta(x - \hat{x}_l(t))\, \delta(y - \hat{y}_l(t)), \quad (12)$$

where $\{p_l(t), l = 1, 2, \ldots, N_p\}$ are the moving loads and they are moving as a group at a fixed spacing. $(\hat{x}_l(t), \hat{y}_l(t))$ is the position of the moving load $p_l(t)$. $\delta(x)$, $\delta(y)$ are the Dirac function. By modal superposition, the displacement of the orthotropic plate can be written as follows:

$$w(x, y, t) = \sum_{m,n} W_{mn}(x, y) q_{mn}(t), \quad (13)$$

where $W_{mn}(x, y) = Y_{mn}(y) \sin(m\pi x/a)$ is the mode shape of the orthotropic plate, and $q_{mn}(t)$ is the corresponding modal co-ordinate.

Substituting equation (13) into equation (12) results in

$$\ddot{q}_{mn}(t) + 2\zeta_{mn}\omega_{mn}\dot{q}_{mn}(t) + \omega_{ij}^2 q_{mn}(t) = \frac{2}{\rho h a \int_0^b Y_{mn}^2(y)\, \mathrm{d}y} \sum_{l=1}^{N_p} p_l(t) Y_{mn}(\hat{y}_l(t)) \sin\left(\frac{m\pi}{a}\hat{x}_l(t)\right)$$
$$(m, n = 1,2, \ldots), \quad (14)$$

where $\zeta_{mn} = (C/2\rho h\omega_{mn})$ and a, b are the dimensions of the orthotropic plate in x and y directions respectively. Equation (14) can be solved in the time domain by the convolution integral with the plate initially at rest, yielding

$$q_{mn}(t) = \frac{1}{M_{mn}} \int_0^t H_{mn}(t - \tau) f_{mn}(\tau)\, \mathrm{d}\tau, \quad (15)$$

where

$$M_{mn} = \frac{\rho h a}{2} \int_0^b Y_{mn}^2(y)\, \mathrm{d}y,$$

$$H_{mn}(t) = \frac{1}{\omega'_{mn}} \mathrm{e}^{-\zeta_{mn}\omega_{mn}t} \sin(\omega'_{mn}t), \quad t \geqslant 0,$$

$$f_{mn}(t) = \sum_{l=1}^{N_p} p_l(t) Y_{mn}(\hat{y}_l(t)) \sin\left(\frac{m\pi}{a}\hat{x}_l(t)\right), \quad (16)$$

$$\omega'_{mn} = \omega_{mn}\sqrt{1 - \zeta_{mn}^2}.$$

Substituting equation (15) into equation (13), the displacement of the orthotropic plate at point (x, y) and time t can be found, as

$$w(x,y,t) = \sum_{m=1}^{\infty}\sum_{n=1}^{\infty} Y_{mn}(y)\sin\left(\frac{m\pi}{a}x\right)\frac{1}{M_{mn}}\int_0^t H_{mn}(t-\tau)f_{mn}(\tau)\,\mathrm{d}\tau. \tag{17}$$

4. MOVING LOAD IDENTIFICATION

4.1. LOAD IDENTIFICATION FROM STRAINS

The strains under the orthotropic plate at point (x, y) and time t are

$$\begin{aligned}
\varepsilon_x(x,y,t) &= z_t\sum_{m=1}^{\infty}\sum_{n=1}^{\infty}\left(\frac{m\pi}{a}\right)^2 Y_{mn}(y)\sin\left(\frac{m\pi}{a}x\right)\frac{1}{M_{mn}}\int_0^t H_{mn}(t-\tau)f_{mn}(\tau)\,\mathrm{d}\tau,\\
\varepsilon_y(x,y,t) &= -z_t\sum_{m=1}^{\infty}\sum_{n=1}^{\infty} Y''_{mn}(y)\sin\left(\frac{m\pi}{a}x\right)\frac{1}{M_{mn}}\int_0^t H_{mn}(t-\tau)f_{mn}(\tau)\,\mathrm{d}\tau,
\end{aligned} \tag{18}$$

where $\varepsilon_x(x, y, t)$, $\varepsilon_y(x, y, t)$ are the strains at the bottom surface of the plate along x and y directions, respectively, and z_t is the distance from the neutral axis to the bottom tension surface. The strains at measuring point (x_s, y_s) can be written in discrete form including the $MM \times NN$ modes along the x and y directions respectively.

$$\begin{aligned}
\varepsilon_x(x_s,y_s,mm) &= z_t\sum_{m=1}^{MM}\sum_{n=1}^{NN}\left(\frac{m\pi}{a}\right)^2 Y_{mn}(y_s)\sin\left(\frac{m\pi}{a}x_s\right)\frac{1}{M_{mn}}\sum_{k=0}^{mm} H_{mn}(mm-k)f_{mn}(k)\Delta t,\\
\varepsilon_y(x_s,y_s,mm) &= -z_t\sum_{m=1}^{MM}\sum_{n=1}^{NN} Y''_{mn}(y_s)\sin\left(\frac{m\pi}{a}x_s\right)\frac{1}{M_{mn}}\sum_{k=0}^{mm} H_{mn}(mm-k)f_{mn}(k)\Delta t\\
&\qquad (s = 1,2,\ldots,N_s;\ mm = 1,2,\ldots,N),
\end{aligned} \tag{19}$$

where Δt is the time step, $(N + 1)$ the number of sampling points, N_s the number of measuring points, and

$$\begin{aligned}
H_{mn}(k) &= \frac{1}{\omega'_{mn}}\,\mathrm{e}^{-\zeta_{mn}\omega_{mn}k\Delta t}\sin(\omega'_{mn}k\Delta t),\\
f_{mn}(k) &= \sum_{l=1}^{N_p} p_l(k\Delta t)Y_{mn}(\hat{y}_l(k\Delta t))\sin\left(\frac{m\pi}{a}\hat{x}_l(k\Delta t)\right)\quad (m = 1,2,\ldots,MM;\ n = 1,2,\ldots,NN).
\end{aligned} \tag{20}$$

Equation (19) is rewritten in matrix form (only the x direction strains are presented since those for the y direction strains are similar)

$$\varepsilon_x = \mathbf{BP}, \tag{21}$$

where ε_x is a $(N * N_s) \times 1$ matrix, $\mathbf{B}$ is a $(N * N_s) \times (N * N_p)$ matrix and $\mathbf{P}$ is a $(N * N_p) \times 1$ matrix,

$$\begin{aligned}
\varepsilon_x &= \{\varepsilon_x(x_1,y_1,1),\varepsilon_x(x_2,y_2,1),\ldots,\varepsilon_x(x_{N_s},y_{N_s},1),\varepsilon_x(x_1,y_1,2),\ldots,\varepsilon_x(x_{N_s},y_{N_s},N)\}^{\mathrm{T}},\\
\mathbf{P} &= \{p_1(0),p_2(0),\ldots,p_{N_p}(0),p_1(1),\ldots,p_{N_p}(N-1)\}^{\mathrm{T}},
\end{aligned} \tag{22}$$

$$\mathbf{B} = \begin{bmatrix} \mathbf{B}_{10} & 0 & \cdots & 0 \\ \mathbf{B}_{20} & \mathbf{B}_{21} & \cdots & 0 \\ \vdots & \vdots & \vdots & \vdots \\ \mathbf{B}_{N0} & \mathbf{B}_{N1} & \cdots & \mathbf{B}_{NN-1} \end{bmatrix}_{(N_s * N) \times (N_p * N)}, \quad \mathbf{B}_{mmk} = \begin{bmatrix} b_{11} & b_{12} & \cdots & b_{1N_p} \\ b_{21} & b_{22} & \cdots & b_{2N_p} \\ \cdots & \cdots & \vdots & \cdots \\ b_{N_s 1} & b_{N_s 2} & \cdots & b_{N_s N_p} \end{bmatrix}_{N_s \times N_p}. \tag{23}$$

$$b_{sl} = z_t \Delta t \sum_{m=1}^{MM} \sum_{n=1}^{NN} \frac{1}{M_{mm}\omega'_{mn}} \left(\frac{m\pi}{a}\right)^2 Y_{mn}(y_s) \sin\left(\frac{m\pi}{a} x_s\right)$$

$$\mathrm{e}^{-\zeta_{mn}\omega_{mn}(mm-k)\Delta t} \sin(\omega'_{mn}(mm-k)\Delta t) Y_{mn}(\hat{y}_l(k\Delta t)) \sin\left(\frac{m\pi}{a}\hat{x}_l(k\Delta t)\right)$$

$$(mm = 1, 2, 3, \ldots, N;\ k = 0, 1, 2, \ldots, N-1;\ s = 1, 2, \ldots, N_s;\ l = 1,2, \ldots, N_p).$$

Since the identified force $\mathbf{P}$ is not a continuous function of the measured data, a regularization method developed by Tiknonov [22] is used to solve this ill-posed problem [23]. The load identification problem can be formulated as the following damped least-squares problem.

$$\min J(\mathbf{P}, \lambda) = (\varepsilon_x - \mathbf{BP}, \mathbf{R}(\varepsilon_x - \mathbf{BP})) + \lambda(\mathbf{P}, \mathbf{P}), \tag{24}$$

where λ is a non-negative regularization parameter in the form of a diagonal matrix. $\mathbf{R}$ is a weight matrix determined from the measured information.

4.2. LOAD IDENTIFICATION FROM ACCELERATIONS

The acceleration at a point (x, y) and time t obtained from equation (17) is

$$\ddot{w}(x, y, t) = \sum_{m=1}^{\infty} \sum_{n=1}^{\infty} Y_{mn}(y) \sin\left(\frac{m\pi}{a} x\right) \frac{1}{M_{mn}} \left[f_{mn}(t) + \int_0^t \ddot{H}_{mn}(t-\tau) f_{mn}(\tau)\, \mathrm{d}\tau \right], \tag{25}$$

where

$$\ddot{H}_{mn}(t) = \frac{1}{\omega'_{mn}} \mathrm{e}^{-\zeta_{mn}\omega'_{mn}t} \{ [(\zeta_{mn}\omega_{mn})^2 - \omega'^2_{mn}] \sin \omega'_{mn} t - 2\zeta_{mn}\omega_{mn}\omega'_{mn} \cos \omega'_{mn} t \}. \tag{26}$$

The acceleration at measuring point (x_s, y_s) can be written in discrete form including the $MM \times NN$ modes as

$$\ddot{w}(x_s, y_s, mm) = \sum_{m=1}^{MM} \sum_{n=1}^{NN} Y_{mn}(y_s) \sin\left(\frac{m\pi}{a} x_s\right) \frac{1}{M_{mn}} \left[f_{mn}(mm) + \sum_{k=0}^{mm} \ddot{H}_{mn}(mm-k) f_{mn}(k)\, \Delta t \right]$$

$$(s = 1, 2, \ldots, N_s;\ mm = 1, 2, \ldots, N), \tag{27}$$

$$\ddot{H}_{mn}(k) = \frac{1}{\omega'_{mn}} \mathrm{e}^{-\zeta_{mn}\omega_{mn}k\Delta t} \{ [(\zeta_{mn}\omega_{mn})^2 - \omega'^2_{mn}] \sin(\omega'_{mn}k\Delta t) - 2\zeta_{mn}\omega_{mn}\omega'_{mn} \cos(\omega'_{mn}k\Delta t) \},$$

$$f_{mn}(k) = \sum_{l=1}^{N_p} p_l(k\Delta t) Y_{mn}(\hat{y}_l(k\Delta t)) \sin\left(\frac{m\pi}{a}\hat{x}_l(k\Delta t)\right)$$

$$(m = 1, 2, \ldots, MM;\ n = 1, 2, \ldots, NN;\ k = 0, 1, 2, \ldots, N-1). \tag{28}$$

Equation (27) can also be written in matrix form as follows:

$$\ddot{\mathbf{w}} = \mathbf{DP}, \tag{29}$$

where

$$\begin{aligned} \ddot{\mathbf{w}} &= \{\ddot{w}(x_1, y_1, 1), \ddot{w}(x_2, y_2, 1), \ldots, \ddot{w}(x_{N_s}, y_{N_s}, 1), \ddot{w}(x_1, y_1, 2), \ldots, \ddot{w}(x_{N_s}, y_{N_s}, N)\}^{\mathrm{T}}, \\ \mathbf{P} &= \{p_1(0), p_2(0), \ldots, p_{N_p}(0), p_1(1), \ldots, p_{N_p}(N-1)\}^{\mathrm{T}}, \end{aligned} \tag{30}$$

$$\mathbf{D} = \begin{bmatrix} \mathbf{D}_{10} & 0 & \cdots & 0 \\ \mathbf{D}_{20} & \mathbf{D}_{21} & \cdots & 0 \\ \vdots & \vdots & \vdots & \vdots \\ \mathbf{D}_{N0} & \mathbf{D}_{N1} & \cdots & \mathbf{D}_{NN-1} \end{bmatrix}_{(N_s * N) \times (N_p * N)}, \quad \mathbf{D}_{mmk} = \begin{bmatrix} d_{11} & d_{12} & \cdots & d_{1N_p} \\ d_{21} & d_{22} & \cdots & d_{2N_p} \\ \cdots & \cdots & \vdots & \cdots \\ d_{N_s 1} & d_{N_s 2} & \cdots & d_{N_s N_p} \end{bmatrix}_{N_s \times N_p},$$

$$d_{sl}^{*} = \Delta t \sum_{m=1}^{MM} \sum_{n=1}^{NN} \frac{1}{M_{mn}\omega'_{mn}} Y_{mn}(y_s) \sin\left(\frac{m\pi}{a} x_s\right) \mathrm{e}^{-\zeta_{mn}\omega_{mn}(mm-k)\Delta t} \{\sin(\omega'_{mn}(mm-k)\Delta t)$$

$$[(\zeta_{mn}\omega_{mn})^2 - \omega'^2_{mn}] - 2\zeta_{mn}\omega_{mn}\omega'_{mn} \cos(\omega'_{mn}(mm-k)\Delta t)\} Y_{mn}(\hat{y}_l(k\Delta t)) \sin\left(\frac{m\pi}{a}\hat{x}_l(k\Delta t)\right)$$

$$(mm = 1, 2, 3, \ldots, N;\ k = 0, 1, 2, \ldots, N-1,\ s = 1, 2, \ldots, N_s;\ l = 1, 2, \ldots, N_p),$$

when $k < mm$, $d_{sl} = d_{sl}^{*}$;
when $k = mm$,

$$d_{sl} = d_{sl}^{*} + \sum_{m=1}^{MM} \sum_{n=1}^{NN} Y_{mn}(y_s) \sin\left(\frac{m\pi}{a}\right) Y_{mn}(\hat{y}_l(mm\Delta t) \sin\left(\frac{m\pi}{a}\hat{x}_l(mm\Delta t)\right) \Big/ M_{mn}. \tag{31}$$

Again the load identification problem is formulated as a damped least-squares problem,

$$\min J(\mathbf{P}, \lambda) = (\ddot{\mathbf{w}} - \mathbf{DP}, \mathbf{R}(\ddot{\mathbf{w}} - \mathbf{DP})) + \lambda(\mathbf{P}, \mathbf{P}). \tag{32}$$

The moving loads are determined from equations (24) and (32) using either strains or accelerations or both. The method to determine the optimal regularization parameter λ is referred to the work by Busby and Trujillo [24].

5. COMPUTATION ALGORITHM

The computational process is implemented as follows:

(1) basing on the maximum exciting frequency generated by the moving loads, the number of mode shapes $MM \times NN$, the number of the measuring points N_s and the sampling frequency are determined;
(2) the natural frequencies ω_{mn} and the mode shapes $W_{mn}(x, y)$ of the orthotropic rectangular plate are calculated according to equation (11);

(3) matrix $\mathbf{B}_{mmk}$ and $\mathbf{D}_{mmk}$ are calculated from equation (23) and (31);
(4) set initial λ equals to zero.
(5) calculate $\mathbf{P}(0)$ from

$$\mathbf{P}(0) = (\mathbf{B}_{10}^{\mathrm{T}}\mathbf{B}_{10} + \lambda I)^{-1}\mathbf{B}_{10}^{\mathrm{T}}\varepsilon_x(1) \quad \text{or} \quad \mathbf{P}(0) = (\mathbf{D}_{10}^{\mathrm{T}}\mathbf{D}_{10} + \lambda I)^{-1}\mathbf{D}_{10}^{\mathrm{T}}\ddot{\mathbf{w}}(1), \tag{33}$$

where

$$\varepsilon_x(j) = \{\varepsilon_x(x_1, y_1, j), \varepsilon_x(x_2, y_2, j), \ldots, \varepsilon_x(x_{N_s}, y_{N_s}, j)\}^{\mathrm{T}},$$

$$\ddot{\mathbf{w}}(j) = \{\ddot{w}(x_1, y_1, j), \ddot{w}(x_2, y_2, j), \ldots, \ddot{w}(x_{N_s}, y_{N_s}, j)\}^{\mathrm{T}} \quad (j = 1, 2, \ldots, N),$$

$$\mathbf{P}(i) = \{p_1(i), p_2(i), \ldots, p_{N_p}(i)\}^{\mathrm{T}} \quad (j = 1, 2, \ldots, N-1);$$

(6) calculate $\mathbf{P}(k)$ from

$$\mathbf{P}(k) = (\mathbf{B}_{(k+1)K}^{\mathrm{T}}\mathbf{B}_{(k+1)k} + \lambda I)\mathbf{B}_{(k+1)k}^{\mathrm{T}}\left(\varepsilon_x(k+1) - \sum_{i=0}^{k-1}\mathbf{B}_{(i+1)i}\mathbf{P}(i)\right) \quad \text{or}$$

$$\mathbf{P}(k) = (\mathbf{D}_{(k+1)K}^{\mathrm{T}}\mathbf{D}_{(k+1)k} + \lambda I)\mathbf{D}_{(k+1)k}^{\mathrm{T}}\left(\ddot{\mathbf{w}}(k+1) - \sum_{i=0}^{k-1}\mathbf{D}_{(i+1)i}\mathbf{P}(i)\right) \tag{34}$$

$$(k = 1, 2, \ldots, N-1);$$

(7) determine the optimal regularization parameter λ by minimizing the function $J(P, \lambda)$ using MATLAB. The moving loads can then be calculated from Steps 5 and 6.

6. VERIFICATION AND DISCUSSIONS

6.1. RELIABILITY OF THE METHOD IN EXPERIMENT

The experimental results obtained for a model car moving on a simply supported beam are used for this study. The experimental set-up is shown diagrammatically in Figure 2. The main beam located in the laboratory is 3678 mm long with 100 mm × 25 mm uniform cross-section. The Young's modulus of material is $2{\cdot}1 \times 10^9$ N/m^2. The mass density is 2300 Kg/m^3, and the Poisson ratio is 0·3. A leading beam for the vehicle to pick up speed and another beam at the other end for receiving the vehicle after its exit from the main beam are also shown. The beams are simply supported and the ends of the beams are placed close together leaving only a very narrow gap of approximately 1 mm. This is necessary in order not to have a large impulsive force on the beam when the wheels cross the gap.

A U-shaped aluminum section on the upper surface of the beams serves as a direction guide for the car. The model car is pulled along the guide by a string wound on a wheel mount on the axle of an electric motor where the rotating speed can be adjusted. Thirteen photoelectric seasons are mounted on the beams to measure and monitor the moving speed of the car.

Seven strain gauges are mounted at the bottom of the main beam to measure the bending moment responses of the beam. A TEAC 14-channel magnetic tape recorder and an 8-channel dynamic testing and analysis system are used for data collection and analysis in the experiment. The sampling frequency is 2000 Hz. The recorded length of each test lasts for 6 s. The model car has two axles at a spacing of 0·557 m and it runs on four steel wheels

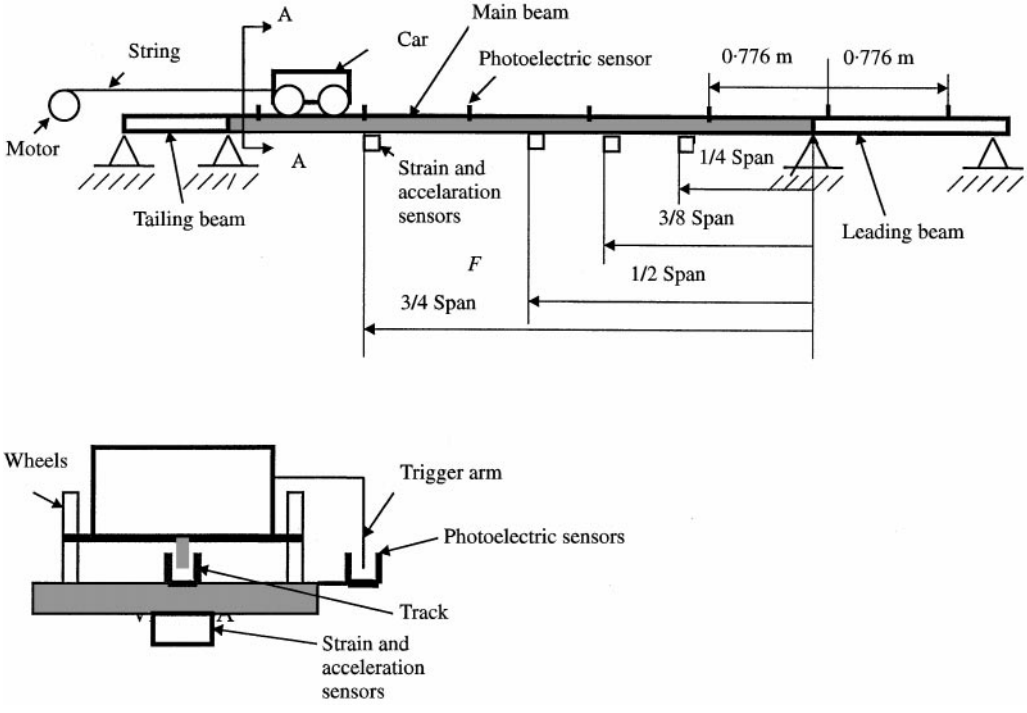

Figure 2. Diagrammatic drawing of the experimental set-up.

with rubber band on the outside. The mass of the whole car is 16·6 kg. The static axle weights are 8·78 and 7·82 kg for the front and rear axles respectively. The transverse spacing between wheels is 0·08 m.

The car is modelled as two-axle forces moving on top of the beam. The beam sub-system has very small damping, and hence the damping coefficient is set to 0·02 in the computation. Figure 3 shows the measuring strains at 1/4L, 1/2L and 3/4L. Since the transverse spacing of the wheels is very small compared with the axle spacing, the identification is in terms of the axle loads instead of the individual wheel loads which are difficult to differentiate. Figure 4 shows the identified axle forces using the beam model [13] and using the plate model described in this paper. The vehicle moves at an average speed of 1·1856 m/s, and the first three modes are used in the identification. There are large fluctuations in the two sets of results especially after the entrance of the second axle and before the exit of the first axle. The two sets of curves are close to the static axle weight with large fluctuations in their histories. The fluctuations are affected by the measurement noise, and therefore whether a beam model can replace a plate model in the analysis or not cannot be ascertained from these results. The following section gives further discussions on the conditions when a plate can be modelled as a beam without introducing significant errors in the identified forces.

6.2. THE BEAM MODEL VERSUS THE PLATE MODEL

A beam model for the bridge deck can be derived from equations (16) and (17). The displacement at a point along the central line of the bridge deck with the loads moving

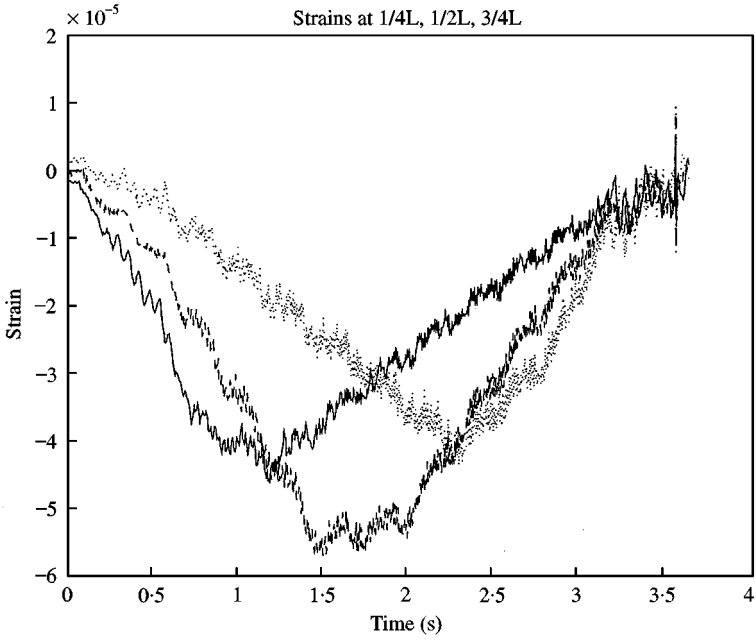

Figure 3. Strains at 1/4L, 1/2L and 3/4L: ——, 1/4L; - - -, 1/2L; ····, 3/4L.

along $y = e$ can be obtained from equation (17) as follows:

$$w\left(x, \frac{b}{2}, t\right) = \sum_{m=1}^{\infty} \sum_{n=1}^{\infty} C_{bmn} \sin\left(\frac{m\pi}{a} x\right) \frac{1}{M_b} \int_0^t H_{mn}(t-\tau) f_{bm}(\tau)\, \mathrm{d}\tau, \tag{35}$$

$$C_{bmn} = \frac{b Y_{mn}(b/2) Y_{mn}(e)}{\int_0^b Y_{mn}^2(y)\, \mathrm{d}y}, \quad M_b = \rho h a b/2, \tag{36}$$

$$f_{bm} = \sum_{l=1}^{N_p} p_1(t) \sin\left(\frac{m\pi}{a} \hat{x}_1(t)\right),$$

where e is the eccentricity of the moving load, and h is the thickness of the beam.

If $n = 1$, i.e., the torsional modes are not considered, equation (35) is the same as that for the displacement of an equivalent beam. Therefore, the identification can be simplified using a beam model when $n = 1$. Table 1 shows the natural frequencies of an isotropic plate with two simply supported edges and two free edges. The length of the plate is 3·678 m and the thickness is 0·025 m. The width of the plate varies from 0·1 to 1·8 m. The lowest several modes of the plates mainly consist of longitudinal modes in the x direction with $n = 1$.

Two constant forces 87·25 and 38·25 N at a fixed spacing of 0·557 m are moving across the plate at 1·0 m/s. The sampling rate is 100 Hz. Figure 5 shows the identified forces from accelerations at 1/4a, 1/2a, 3/4a and 1/2b of a 0·1 and 0·4 m wide plate using the beam and the plate models, and the lowest three modes with $n = 1$ are used. The resulting curves for the two-plate models overlap and exactly match those of the true forces without error. The three sets of curves are very close to each other except near the start and end of the time histories. The plate model can exactly identify the forces using the proposed method, while

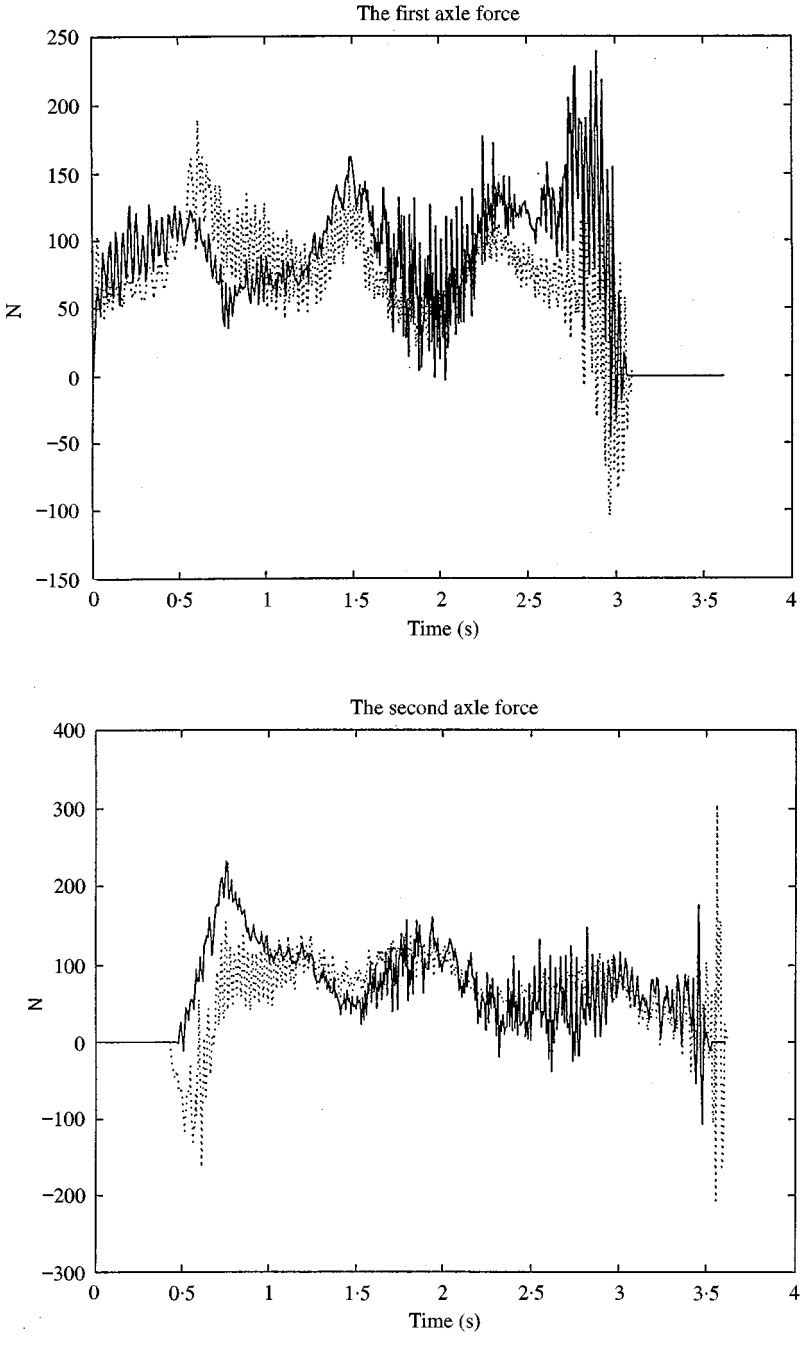

Figure 4. Identified forces by beam model and plate model: ——, beam model; - - -, plate model.

results from the beam models deteriorates for a larger width of the plate used in the model. The modal frequencies in Table 1 indicate that the beam model would be accurate enough for identifying the moving loads when the highest natural frequency of the plate with $n = 1$, is larger than the frequencies used in the identification.

TABLE 1

Natural frequencies (Hz) of beam and plate with different width

Width of plate		Mode type	*x*-mode no. 1	2	3	4	5	6
Beam model (0·1 m width)		B	4·32	17·27	38·86	69·08	107·94	155·43
Plate model	0·1 m	B	4·22	16·89	38·01	67·59	105·66	152·23
	0·2 m	B	4·22	16·90	38·07	67·76	106·03	152·94
		first T	—	—	—	—	107·54*	—
	0·3 m	B	4·22	16·92	38·14	67·97	106·50	153·80
		first T	—	—	—	71·77*	144·35*	—
	0·4 m	B	4·23	16·94	38·24	68·23	107·01	154·68
		first T	—	—	53·91*	—	108·89*	—
	1·8 m	B	4·27	17·35	39·38	70·36	110·29	159·17
		first T	12·72*	29·68*	51·57*	85·26*	125·55*	—
		second T	—	—	53·46*	97·36*	128·93*	—
		third T	—	—	70·22*		132·16*	—
		fourth T	—	—	—	—	146·95*	—

*Denotes the natural frequency corresponds to mode shape mainly in the *y* direction (B: bending mode; second T: second torsional mode).

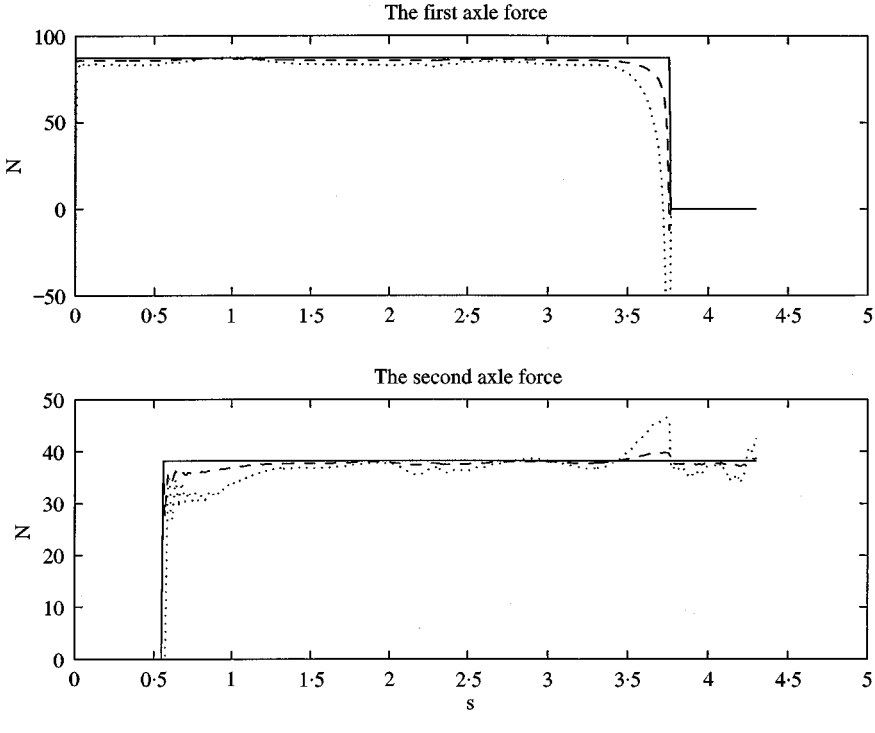

Figure 5. Identified forces by beam model and plate model: ——, plate model; - - -, beam model (0·1 m wide); ····, beam model (0·4 m wide).

6.3. TWO MOVING LOADS IDENTIFICATION WITH PLATE MODEL

A diagrammatic cross-section of a simply supported beam-slab-type bridge deck is shown in Figure 6. The parameters of the bridge deck are listed as follows: $a = 20\,\text{m}$, $b = 11\,\text{m}$, $E = 2{\cdot}1 \times 10^9\,\text{N/m}^2$, $\rho = 2300\,\text{kg/m}^3$. For I-beam: $I = 0{\cdot}118\,\text{m}^4$, $J = 0{\cdot}04385\,\text{m}^2$, top slab thickness $= 0{\cdot}2\,\text{m}$, depth of girder $= 1{\cdot}13\,\text{m}$.

The two moving loads to be identified are

$$p_1(t) = 150\,000(1 + 0{\cdot}1 \sin 10\pi t + 0{\cdot}05 \sin 40\pi t)\ \text{N},$$

$$p_2(t) = 150\,000(1 - 0{\cdot}1 \sin 10\pi t + 0{\cdot}05 \sin 50\pi t)\ \text{N}.$$

Note that there is an out-of-phase component in the forces simulating the pitching motion of a vehicle. White noise is added to the calculated displacements due to the moving loads to simulate the polluted measurement as

$$\ddot{w} = \ddot{w}_{calculated}(1 + E_p N_{oise}),$$

$$\varepsilon = \varepsilon_{calculated}(1 + E_p N_{oise}),$$

where $\ddot{w}$, ε are the measured accelerations and strains used for the identification, E_P is the noise level, N_{oise} is a standard normal distribution vector (with zero mean value and unit standard deviation). $\ddot{w}_{calculated}$, $\varepsilon_{calculated}$ are the calculated accelerations and strains. The errors in the simulating results are calculated from the following equation:

$$S = \frac{\|P_{identified} - P_{True}\|}{\|P_{True}\|} \times 100\%.$$

Calculations are made for the loads moving at a fixed spacing of 4 m along the central line and along $y = 3/8b$. The moving speed is 10 m/s and the sampling rate is 100 Hz. The lowest nine vibration modes are used in the simulation, and nine measurement points are located at 1/4a, 1/2a and 3/4a on the second, third and the fourth I-beams. The number of the measuring points is taken equal to the number of the vibration modes [13].

Figure 7 shows the identified results moving along the central line from the accelerations and the strains with 1% noise level. Very good results are achieved except at the start and end of the time histories. There is a large deviation between the true load and the curves

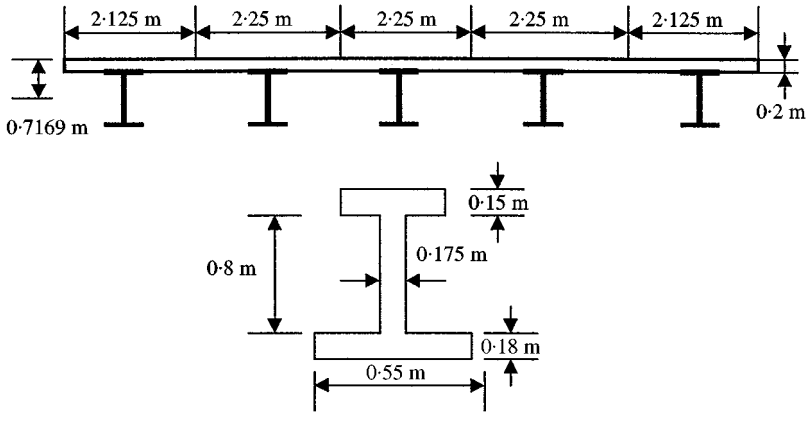

Figure 6. A simply supported beam-slab bridge deck.

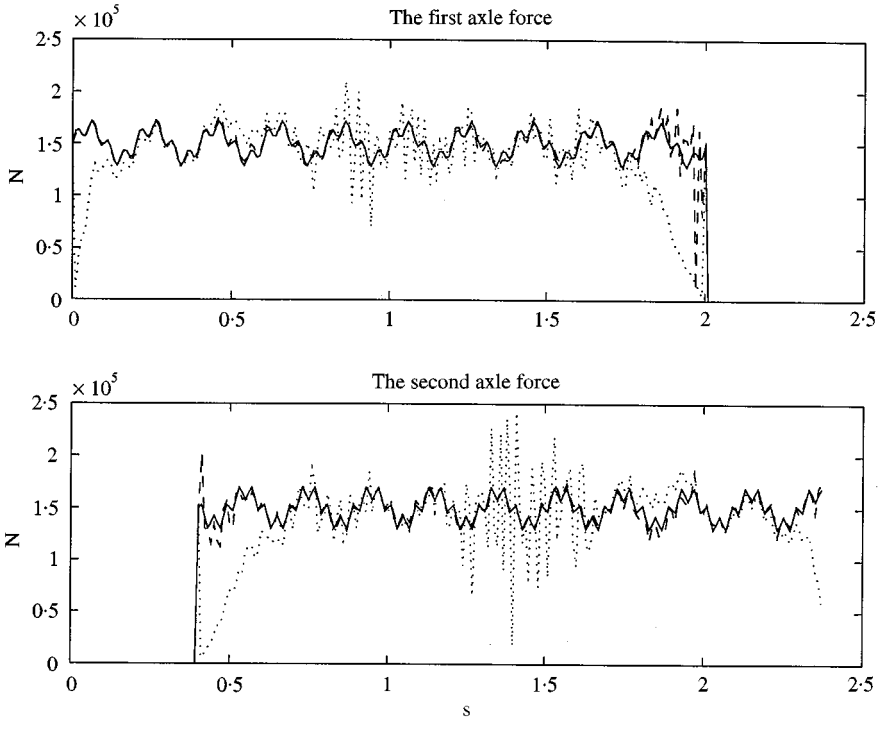

Figure 7. Identified forces from accelerations and strains: ——, true load; - - -, acceleration; ····, strains.

TABLE 2

Errors in the identified forces with different noise levels

Eccentricity	Responses	N_{oise}(%)	λ	First force (%)	Second force (%)
0	Acceleration	1	$4{\cdot}29 \times 10^{-13}$	2·74	2·53
		5	$4{\cdot}96 \times 10^{-11}$	12·30	11·25
		10	$1{\cdot}26 \times 10^{-10}$	18·97	17·81
	Strain	1	$1{\cdot}23 \times 10^{-21}$	15·92	17·69
		5	$1{\cdot}31 \times 10^{-20}$	27·44	29·42
		10	$2{\cdot}44 \times 10^{-20}$	34·71	37·00
1/8b	Acceleration	1	$1{\cdot}60 \times 10^{-12}$	4·30	4·16
		5	$5{\cdot}51 \times 10^{-11}$	15·29	14·20
		10	$1{\cdot}17 \times 10^{-10}$	22·44	21·24
	Strain	1	$1{\cdot}22{\cdot} \times 10^{-21}$	16·60	18·48
		5	$1{\cdot}17 \times 10^{-20}$	28·51	30·48
		10	$2{\cdot}21 \times 10^{-20}$	35·97	38·13

from strain when the load is near the mid-span of the beam. This is due to the noise effect that increases with the large strain responses when the load is at mid-span. The observation contrasts with the identified results when there is no noise in the responses and the identified forces exactly match those of the true forces. The curves from acceleration exhibit no such large differences, because the acceleration responses remain relatively stable throughout the duration. Those from accelerations almost match the true curves perfectly. Table 2 shows the errors in the identified forces with no smoothing on data at different noise levels.

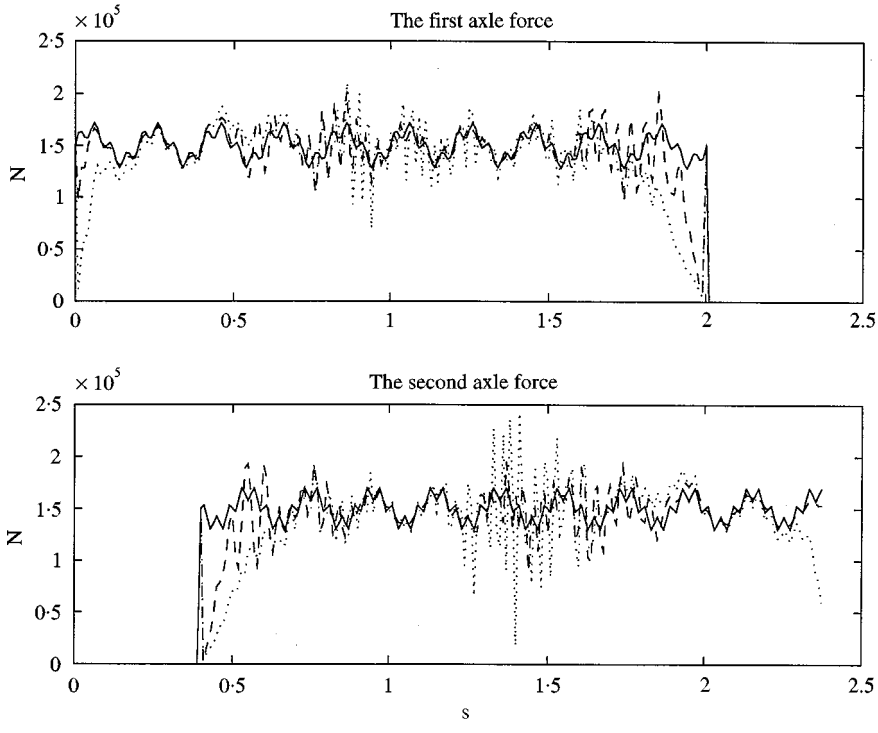

Figure 8. Identified forces from strains with or without smoothing: ——, true load; - - -, smoothing; ····, no smoothing.

Accelerations give much better results than strains at different noise levels, and the identification of eccentric load using this set of sensors gives slightly larger errors than the loads along the central line. This may be due to the smaller responses at the sensor locations caused by the eccentric loads. Further work has to be done on the best sensor locations for identifying loads moving on different paths.

Figure 8 shows the identified loads moving along the central line from the strains only with or without three-points smoothing on the measured data with 1% noise level. It is seen that smoothing before the identification can improve the results significantly specially on the variation in the middle of the time histories. This variation is due to the low response when the force traverses the mid-span of the structure where the second longitudinal modes responses are smallest. Table 3 also shows reduction in the errors over the whole time period when smoothing is used. The improvement is larger in the strains than the accelerations.

7. CONCLUSIONS

A method to estimate loads moving on top of a bridge deck using the measured structural responses is presented. The bridge deck is represented by an orthotropic plate model and Tikhonov regularization technique is used to provide bounds to the identified forces. The simulation and laboratory results show that

(1) The method proposed in the paper is effective to identify the moving loads from the responses of the bridge deck, and acceptable results can be obtained either from the

TABLE 3

Errors in the identified forces with or without smoothing

	Responses	N_{oise}(%)	λ	First force (%)	Second force (%)
No smoothing	Acceleration	1	$4{\cdot}29 \times 10^{-13}$	2·74	2·53
		5	$4{\cdot}96 \times 10^{-11}$	12·30	11·25
		10	$1{\cdot}26 \times 10^{-10}$	18·97	17·81
	Strain	1	$1{\cdot}23 \times 10^{-21}$	15·92	17·69
		5	$1{\cdot}31 \times 10^{-20}$	27·44	29·42
		10	$2{\cdot}44 \times 10^{-20}$	34·71	37·00
Smoothing	Acceleration	1	$1{\cdot}22 \times 10^{-20}$	2·72	3·14
		5	$2{\cdot}80 \times 10^{-12}$	9·24	9·43
		10	$6{\cdot}63 \times 10^{-11}$	13·59	13·59
	Strain	1	$7{\cdot}57 \times 10^{-23}$	9·07	10·06
		5	$1{\cdot}84 \times 10^{-21}$	18·60	20·51
		10	$6{\cdot}38 \times 10^{-21}$	24·76	27·01

accelerations or the strains, but acceleration measurements would provide better results than those from strain measurements. Identification of forces moving on an eccentric path in slightly less accurate than that for forces moving along the central line of the bridge deck when the sensors are around the middle of the bridge cross-section.

(2) When the measuring noise is very large, pre-processing procedures are required to reduce the measurement noise in the responses before the regularization method can work effectively to provide bounds to the identified forces.

(3) When the lower modes of the bridge deck are dominated by vibration modes along the longitudinal axis, a beam model instead of a plate mode may be accurate enough in the identification.

ACKNOWLEDGMENT

The work described in this paper was supported by a grant from the Hong Kong Polytechnic University Research Funding Project No. V653.

REFERENCES

1. R. CANTINENI 1992 *Swiss Federal Laboratories for Materials Testing and Research* (*EMPA*) *Report No*. 220, 240p. Dynamic behaviour of highway bridges under the passage of heavy vehicles.
2. R. J. HEYWOOD 1994 *International Journal of Vehicle Design*. Influence of truck suspensions on the dynamic response of a short span bridge.
3. M. F. GREEN and D. CEBON 1994 *Journal of Sound and Vibration* **170**, 51–78. Dynamic response of highway bridges to heavy vehicle loads: theory and experimental validation.
4. Y. B. YANG and J. D. YAU 1997 *Journal of Structural Engineering*, *ASCE* **123**, 1512–1518. Vehicle–bridge interaction element for dynamic analysis.
5. K. HENCHI, M. FAFARD, M. TALBOT and G. DHATT 1998 *Journal of Sound and Vibration* **212**, 663–683. An efficient algorithm for dynamic analysis of bridges under moving vehicles using a coupled modal and physical components approach.
6. R. J. PETERS 1984 *Proceedings of* 12*th ARRB Conference*, Vol. **12**, 10–18. A system to obtain vehicle axle weights.

7. R. J. PETERS 1986 *Proceedings of 13th ARRB and 5th REAAA Combined Conference*, Part 6, 70–83. An unmanned and undetectable highway speed vehicle weighing system.
8. C. O'CONNOR and T. H. T. CHAN 1988 *Journal of Structural Engineering ASCE* **114**, 1703–1723. Dynamic wheel loads from bridge strains.
9. S. S. LAW, T. H. T. CHAN and Q. H. ZENG 1997 *Journal of Sound and Vibration* **201**, 1–22. Moving force identification: a time domain method.
10. S. S. LAW, T. H. T. CHAN and Q. H. ZENG 1999 *Journal of Dynamic Systems, Measurement and Control ASME* **12**, 394–401 Moving force identification: a frequency and time domains analysis.
11. T. H. T. CHAN, S. S. LAW, T. H. YUNG and X. R. YUAN 1999 *Journal of Sound and Vibration* **219**, 503–524. An interpretive method for moving force identification.
12. S. S. LAW and Y. L. FANG *Journal of Sound and Vibration, ASCE*. Moving force identification: optimal state estimation approach (accepted).
13. X. Q. ZHU and S. S. LAW 1999 *Journal of Sound and Vibration* **228**, 377–396. Moving forces identification on a multi-span continuous bridge.
14. B. BAKHT and L. G. JAEGER 1985 *Bridge Analysis Simplified*. New York: McGraw-Hill.
15. L. FRYBA 1972 *Vibration of Solids and Structures under Moving Loads*. Groningen: Noordoff.
16. J. S. WU, M. L. LEE and T. S. LAI 1987 *International Journal for Numerical Methods in Engineering* **24**, 743–762. The dynamic analysis of a flat under a moving load by the finite element method.
17. R.-T. WANG and T. Y. LIN 1996 *Journal of Chinese Institute of Engineers* **19**, 467–477. Vibration of multi-span Mindlin plates to a moving load.
18. S. MARCHESIELLO, A. FASANA, L. GARIBALDI and B. A. D. PIOMBO 1999 *Journal of Sound and Vibration* **224**, 541–561. Dynamics of multi-span continuous straight bridges subject to multi-degrees of freedom moving vehicle excitation.
19. T. H. T. CHAN and J. H. F. CHAN 1999 *Structural Engineering and Mechanics* **8**, 85–102. The use of eccentric beam elements in the analysis of slab-on-girder bridges.
20. X. Q. ZHU and S. S. LAW 1999 *Journal of Structural Engineering, ASCE*. Dynamic behavior of orthotropic plates under moving loads (under review).
21. N. J. HUFFINGTON and W. H. HOPPMANN II 1958 *Journal of Applied Mechanics ASME* **25**, 389–395. On the transverse vibrations of rectangular orthotropic plates.
22. A. N. TIKHONOV 1963 *Soviet Mathematics* **4**, 1035–1038. On the solution of ill-posed problems and the method of regularization.
23. V. A. MOROZOV 1984 *Methods for Solving Incorrectly Posed Problems*, 1–64. Berlin: Springer-Verlag.
24. H. R. BUSBY and D. M. TRUJILLO 1997 *Computers and Structures* **63**, 243–248. Optimal regularization of an inverse dynamic problem.

APPENDIX A. FORMULATION OF COEFFICIENTS a_{ij}

The coefficients a_{ij} stated in equation (11) are listed as follows:
When $D_x < \rho h \omega_{mn}^2 (a/m\pi)^4$,

$$a_{11} = 0, \quad a_{12} = r_{2mn}^2 - v\left(\frac{m\pi}{a}\right)^2, \quad a_{13} = 0, \quad a_{14} = -r_{1mn}^2 - v\left(\frac{m\pi}{a}\right)^2,$$

$$a_{21} = a_{12}\sin(r_{2mn}b), \quad a_{22} = a_{14}\sinh(r_{1mn}b),$$

$$a_{23} = a_{12}\cos(r_{2mn}b), \quad a_{24} = a_{14}\cosh(r_{1mn}b),$$

$$a_{31} = D_y r_{2mn}^3 + (D_{xy} + 2D_k)\left(\frac{m\pi}{a}\right)^2 r_{2mn}, \quad a_{32} = 0,$$

$$a_{33} = -D_y r_{1mn}^3 + (D_{xy} + 2D_k)\left(\frac{m\pi}{a}\right)^2 r_{1mn}, \quad a_{34} = 0,$$

$$a_{41} = a_{31}\cos(r_{2mn}b), \quad a_{42} = -a_{31}\sin(r_{2mn}b),$$

$$a_{43} = a_{33}\cosh(r_{1mn}b), \quad a_{44} = a_{33}\sinh(r_{1mn}b).$$

When $D_{xy}^2/D_y + \rho h\omega_{mn}^2(a/m\pi)^4 > D_x > \rho h\omega_{mn}^2(a/m\pi)^4$,

$$a_{11} = 0, \quad a_{12} = r_{1mn}^2 - v\left(\frac{m\pi}{a}\right)^2, \quad a_{13} = 0, \quad a_{14} = r_{3mn}^2 - v\left(\frac{m\pi}{a}\right)^2,$$

$$a_{21} = a_{12}\sinh(r_{1mn}b), \quad a_{22} = a_{12}\cosh(r_{1mn}b),$$

$$a_{23} = a_{14}\sinh(r_{3mn}b), \quad a_{24} = a_{14}\cosh(r_{3mn}b),$$

$$a_{31} = -D_y r_{1mn}^3 + (D_{xy} + 2D_k)\left(\frac{m\pi}{a}\right)^2 r_{1mn}, \quad a_{32} = 0,$$

$$a_{33} = -D_y r_{3mn}^3 + (D_{xy} + 2D_k)\left(\frac{m\pi}{a}\right)^2 r_{3mn}, \quad a_{34} = 0,$$

$$a_{41} = a_{31}\cosh(r_{1mn}b), \quad a_{42} = a_{31}\sinh(r_{1mn}b),$$

$$a_{43} = a_{33}\cosh(r_{3mn}b), \quad a_{44} = a_{33}\sinh(r_{3mn}b).$$

When $D_x > D_{xy}^2/D_y + \rho h\omega_{mn}^2(a/m\pi)^4$,

$$a_{11} = r_{4mn}^2 - r_{5mn}^2 - v\left(\frac{m\pi}{a}\right)^2, \quad a_{12} = 0, \quad a_{13} = 0, \quad a_{14} = 2r_{4mn}r_{5mn},$$

$$a_{21} = a_{11}\cosh(r_{4mn}b)\cos(r_{5mn}b) - 2r_{4mn}r_{5mn}\sinh(r_{4mn}b)\sin(r_{5mn}b),$$

$$a_{22} = a_{11}\cosh(r_{4mn}b)\sin(r_{5mn}b) + 2r_{4mn}r_{5mn}\sinh(r_{4mn}b)\cos(r_{5mn}b),$$

$$a_{23} = a_{11}\sinh(r_{4mn}b)\cos(r_{5mn}b) - 2r_{4mn}r_{5mn}\cosh(r_{4mn}b)\sin(r_{5mn}b),$$

$$a_{24} = a_{11}\sinh(r_{4mn}b)\sin(r_{5mn}b) + 2r_{4mn}r_{5mn}\cosh(r_{4mn}b)\cos(r_{5mn}b),$$

$$a_{31} = 0, \quad a_{32} = (D_{xy} + 2D_k)\left(\frac{m\pi}{a}\right)^2 r_{4mn} - 3D_y r_{4mn}^2 r_{5mn} + D_y r_{5mn}^3,$$

$$a_{33} = -D_y r_{4mn}^3 + (D_{xy} + 2D_k)\left(\frac{m\pi}{a}\right)^2 r_{4mn} + 3D_y r_{5mn}^2 r_{4mn}, \quad a_{34} = 0,$$

$$a_{41} = a_{33}\sinh(r_{4mn}b)\cos(r_{5mn}b) - a_{32}\cosh(r_{4mn}b)\sin(r_{5mn}b),$$

$$a_{42} = a_{33}\sinh(r_{4mn}b)\sin(r_{5mn}b) + a_{32}\cosh(r_{4mn}b)\cos(r_{5mn}b),$$

$$a_{43} = a_{33}\cosh(r_{4mn}b)\cos(r_{5mn}b) - a_{32}\sinh(r_{4mn}b)\sin(r_{5mn}b),$$

$$a_{44} = a_{33}\cosh(r_{4mn}b)\sin(r_{5mn}b) + a_{32}\sinh(r_{4mn}b)\cos(r_{5mn}b),$$

APPENDIX B. NOMENCLATURE

D_x, D_y	flexural rigidities in the x and y directions respectively
E_x, E_y	Young's moduli of orthotropic material in the x and y directions respectively
G_{xy}	shear modulus of orthotropic plate
a, b, h	length, width and thickness of the orthotropic plate
e	eccentricity of moving load
h_e	equivalent thickness of plate
D_{xy}	torsional rigidity
D_k	twisting rigidity of the orthotropic plate
C	damping coefficient of the plate
$w(x, y, t)$	displacement of the orthotropic plate
$\ddot{w}(x, y, t)$	acceleration responses of the orthotropic plate
$W_{ij}(x, y)$	vibration mode shape of the orthotropic plate
$P_i(t)$	the ith moving load
$\hat{x}_i(t), \hat{y}_i(t)$	location of the ith moving load
z_t	is the distance from the neutral axis to the bottom tension surface
N_p	number of moving loads
N_s	number of measuring points
$N + 1$	number of sampling points
$q_{ij}(t)$	modal co-ordinate
$\mathbf{M}, \mathbf{K}, \mathbf{C}$	mass, stiffness, and damping matrices of the orthotropic plate
$Y_{ij}(y)$	mode shape
$Y_{ij}^{(4)}(y), Y_{ij}^{(2)}(y)$	fourth and second derivatives of $Y_{ij}(y)$
I	moment of inertia of I-beam
$A_{ij}, B_{ij}, C_{ij}, D_{ij}$	mode parameters
MM, NN	number of vibration modes along the x and y directions respectively
$\varepsilon_x(x, y, t)$	strains under the orthotropic plate in x direction
$\varepsilon_y(x, y, t)$	strains under the orthotropic plate in y direction
ρ	mass density of the orthotropic plate material
v_{xy}, v_{yx}	the Poisson ratio
ω_{ij}	circular frequency, rad/s
θ	initial phase angle
$\delta(x)$, $\delta(y)$	Dirac function
λ	regularization parameter